UILU-ENG 83-3603

FCP Report No. 47

FATIGUE CRACK GROWTH IN NODULAR CAST IRON

by

Changtsan Hua
Department of Mechanical and Industrial Engineering
University of Illinois at Urbana-Champaign
Urbana, IL 61801

ABSTRACT

The morphology of the graphite in nodular iron significantly influences the mechanical properties. This paper mainly involves the observation of crack growth in nodular iron. An elastic-plastic fracture mechanics parameter ΔJ was used to correlate the crack growth data. The ΔJ parameter was refined by the formula that was proposed by Shih and Hutchinson. A material constant for short cracks that was proposed by Haddad, Smith, and Topper was adopted in this study. Load control tests were conducted in addition to strain control tests to determine the applicability of the model to various loading modes.

A report of the

Fracture Control Program
College of Engineering
University of Illinois at Urbana-Champaign
Urbana, IL 61801

February 1983

ACKNOWLEDGEMENT

This investigation was conducted in the Materials Engineering Research Laboratory, University of Illinois at Urbana-Champaign.

Professor Darrell F. Socie is gratefully acknowledged for his helpful advice. The author is also indebted to Messrs. James Fash, Peter Kurath, and Huseyin Sehitoglu for their many valuable suggestions and assistance throughout the program. The staff of the Department of Mechanical and Industrial Engineering Publications Office is thanked for their assistance in preparing the report.

CONTENTS

LIST OF TABLES

LIST OF FIGURES

INTRODUCTION

Nodular iron has had widespread use since its introduction nearly 40 years ago. Of the various materials used to make foundry products, each is distinguished by special properties. For instance, steel is strong; malleable iron is tough; white iron is hard; gray iron is relatively inexpensive. The uniqueness of nodular iron is that it combines virtually all of these properties.

Many highly stressed parts are now being regularly cast in nodular iron. The irons may be alloyed or heat treated to provide tensile strengths of 400 to 1,400 Mpa with yielded strengths of 270 to 1,100 Mpa and elogation up to 30 percent [1].

Gilbert studied stress/strain properties of nodular iron in tension and compression in 1964 [2]. The morphology of the graphite in cast iron significantly influences the mechanical properties. The amount, size, and configuration of the graphite constituent and its interaction with the matrix structures largely determine the performance of cast irons under most stress conditions. Thus Ikewa and Ohira [3] in 1967 compared the fatigue properties of cast irons with different graphite morphologies and concluded that nodular iron exhibited the best fatigue properties among cast irons.

The failure mechanism in nodular iron has been the subject of much research. Testin [4] proposed that failure related cracks initiate from the most severe flaw such as microshrinkage cavities, slag inclusions, or porosity. The studies by Ikawa and Ohira [3] showed that initiation of cracks occured at the edges of graphite flakes in gray iron or at the periphery of graphite nodules in nodular iron. Fuller [5] observed that changes in graphite form to non-spheroidal shapes would be expected to establish planes of weakness in the structure. Weakening of the structure would cause early

initiation. Mitchell [6] observed that the largest and most severe stress intensifier at or near the surface controls the behavior. It may be a nodular, porosity or in the case of inadequate or improper inoculation, complete spheroidization of the graphite will not occur and "exploded" graphite, more representative of the flakes, will result.

According to previous studies [7,8], up to 95 percent of the fatigue life of gray iron and compacted graphite iron is spent in crack propagation. Similar observations were made for nodular iron by Starkey and Irving [9]. These observations imply that use of a crack initiation model cannot adequately describe the accumulation of damage in cast irons.

This paper mainly involves the observation of crack growth in nodular iron. An elastic-plastic fracture mechanics parameter ΔJ was used to correlate the crack growth data. In an effort to obtain insight into the applicability of ΔJ parameter, an extension of Starky-Irving's work was made. The ΔJ parameter was refined by the formula that was proposed by Shih and Hutchinson [10]. A material constant for short cracks that was proposed by Haddad, Smith, and Topper [11] was adopted in this study. Load control tests were conducted in addition to strain control tests to determine the applicability of the model to various loading modes.

2. J INTEGRAL AS A FATIGUE CRACK GROWTH MODEL

2.1 Background

Research in fatigue crack propagation has been increasing steadily with the development of improved methods for detecting cracks and for monitoring and predicting their growth. In many cases, a large portion of the total service life of a component may be spent in crack propagation. Cast components may contain flaws from the manufacturing process.

A variety of empirical crack growth expressions have been proposed which relate crack growth rate, da/dN, to applied stress and crack length. One of the most important contributions to the study of fatigue crack propagation was done by Paris [12]. Paris proposed that crack growth rate data could be correlated with stress intensity range ΔK, in the following form

$$da/dN = C(\Delta K)^m. \qquad (1)$$

Following Paris's proposal, numerous fatigue propagation laws have been proposed. Most analytical approaches to the problem have attempted to relate the growth rate (da/dN) with crack length, plastic zone size, material constants, stress, and specimen dimensions. The relationships differ primarily in the emphasis placed on the variables and the accompanying assumptions. Unfortunately, the above proposals applied only to linear elastic stress and strain fields. Since the stress-strain response of nodular iron was substantially plastic, the approach of elastic-plastic regime should be employed. In 1968, Rice [13] proposed an independent integral to solve elastic-plastic stress and strain fields.

2.2 Formulation of ΔJ

Several assumptions are made before derivating ΔJ:

(1) The smooth bar fatigue specimen can be represented as a semi-infinite space containing a small edge crack. This assumption will be valid for small cracks.

(2) Crack growth occurs during the entire fatigue life, initiating from a stress intensifier on the first loading and terminates at an arbitrary size macrocrack.

(3) ΔJ only defines the stress and strain fields near the crack tips during the loading half of the cycle despite intermittent unloading [14,15].

(4) Without accounting for crack closure effects, the entire portion of the hysteresis loop is used to estimate ΔJ.

(5) The J solution may be approximated by simply adding the separately computed elastic and plastic solution [10,16].

(6) The ratio of surface crack length to crack depth is 3 and remains constant. The details of this assumption are described in Section 6.

By definition, the compliance form of J is given by [13]

$$J = -\frac{1}{B}\left(\frac{\partial U}{\partial a}\right). \qquad (2)$$

where B = specimen thickness;

U = potential energy per unit length; and

a = crack length.

The solution for an uniformly strain strip containing a semi-infinite crack is

$$J = W^{\infty} h \tag{3}$$

where W^{∞} = remote strain energy density and

h = strip height.

Begley, et al. [17], reasoned that the characteristic length parameter is crack length rather than strip height. That is,

$$J \propto W^{\infty} a. \tag{4}$$

The elastic component of J value can be obtained from the linear stress intensity factor [15]:

$$Je = K^2/E. \tag{5}$$

For edge embedded circular crack [18], the stress intensity factor is given by

$$K = FS\ (\pi a)^{1/2} \tag{6}$$

where F = geometry factor = 1.12 * $2/\pi$. Substitute Eq. (6) into Eq. (5)

$$Je = \frac{F^2 S^2\ \pi a}{E} = F^2 * 2\pi * \frac{S^2}{2E} * a$$

$$= F^2\ 2\pi\ W_e^{\infty} a. \tag{7}$$

The plastic component of J value has been suggested by Shih and

Hutchinson [10]

$$Jp = F^2 f(n)\ (1 + n)\ W_p^{\infty} a \tag{8}$$

where n = cyclic hardening exponent,

$f(n)$ = function of hardening exponent = $3.85\ (1/n)^{1/2}\ (1-n) + \pi n$,

$W_p^{\infty} = s e_p/(1+n)$, and

e_p = plastic strain.

Combining Eqs. (7) and (8), J = Je + Jp when applied to fatigue $J \rightarrow \Delta J$ and $W \rightarrow \Delta W$.

$$\Delta J = \Delta J_e + \Delta J_p = F^2 2\pi\ \Delta\ W_e^{\infty} a + F^2\ f(n)\ (1 + n)\ \Delta W_p^{\infty} a$$

$$= F^2 a\ \Delta S\ [\frac{\pi \Delta S}{E} + (\Delta e - \frac{\Delta S}{E})\ f(n)] \tag{9}$$

where $\Delta e = \Delta e_e + \Delta e_p$,

Δe_e = elastic strain range,

Δe_p = plastic strain range.

Dowling [14] suggested that the lack of correlation for cracks smaller than 0.18 mm may be due to the continuum nature of fracture mechanics. Later the modification of crack length was proposed by El Haddad, et al. [11], in 1978. They proposed that a material constant be included in the elastic-plastic solution for short cracks. The definition of the material constant is

$$a_o = (\frac{\Delta K_{th}}{\Delta \sigma_e})^2\ \frac{1}{\pi} \tag{10}$$

where ΔK_{th} = threshold stress intensity range and

$\Delta\sigma_e$ = fatigue limit range. Then Eq. (9) can be modified to

$$\Delta J = F^2(a + a_o)\ \Delta S\ \left[\frac{\pi\Delta S}{E} + (\Delta e - \frac{\Delta S}{E})\ f(n)\right]. \qquad (11)$$

3. MATERIAL DESCRIPTION AND SPECIMEN PREPARATION

The materials used in this investigation were provided by International Harvester Company. They were casted as Y-block and machined off the upper part. Figure 1 shows microstructures of this iron. As cast, it usually has a microstructure of graphite nodules encased in envelopes of free ferrite (bull's-eye structure), all in a matrix of pearlite (ASTM-A247, Size 5). Material compositions are given in Table 1.

Smooth, cylindrical specimens were machined from the as-cast blocks. Before machining, every block was checked by x-ray radiographs to assure that no significant defects were inside. The dimensions of the specimens are shown in Fig. 2. A standard surface finish was attained for specimen. This degree of finishing was sufficient for monotonic and base line fatigue tests, however, a finer polish was required in order to obtain a clear resolution for crack growth observations. These specimens, while being rotating on a lathe, were polished with a pneumatic rotary polishing rod wrapped with emery paper and felt. Rough polishing was done with emery paper, followed by the felt saturated with 0.3 micron alumina metallographic powder in water.

4. TEST PROGRAM

Material testing was accomplished by a MTS-Computer-based system. This specimen consists of a ±20 kip close loop servohydraulic test frame interfaced with a multiuser digital computer, all tests were computer controlled. Stress-strain data was digitized and stored on floppy disks.

4.1 Monotonic Tests

Monotonic tension tests were performed on nodular iron. An axial extensometer was used to monitor and record the material response.

4.2 Fatigue Baseline Tests

Constant amplitude, completely reversed, strain-controlled (or load-controlled) uniaxial fatigue tests were performed on the specimens. The material was tested at five different strain (or stress) amplitudes, with two or three specimens tested at each amplitude. An axial extensometer was used to monitor and record cyclic response. Fatigue failure was defined as the complete separation of the smooth specimens into two pieces.

4.3 Fatigue crack growth tests

Replicating technique was employed to detect the crack growth. This technique has been used to successfully monitor the development of crack systems. The replicating procedure is as follows:

Acetyl cellulose film (0.034 mm thick) was used to obtain a reproduction of the specimen surface. A replica was obtained by the injection of methyl acetone via syringe into the pocket formed between specimen surface and a strip of film. The dried replica can then be removed and quickly placed between microscope slides. Surface replicas were taken at approximately every

10 percent of expected life which was estimated from base line data. Peak stress (or strain) amplitude was continuously monitored. If an increase of 1 to 2 percent of strain amplitude (stress controlled) or a decrease of 1 to 2 percent of load amplitude (strain controlled) was observed prior to the expected 10 percent increment in life, the test was stopped and a replica was taken to detect the onset of unstable crack propagation. When restarting the test, the previous maximum value of peak strain (or peak stress) was taken as the next reference value.

Observation of the finished replica was accomplished with the aid of an optical microscope. Development of the crack system could be recorded by tracing backwards from the photo depicting the crack near final failure to replicas taken at successively earlier stage in the life.

5. RESULTS

Monotonic tension properties are given in Table 2. Figure 3 illustrates montonic and cyclic stress-strain response of the material. Table 3 summarizes the data for completely reversed load-controlled tests. The results of completely reversed strain-controlled tests are given in Table 4. Stress-life data and strain life data are given in Figs. 4 and 5, respectively. Through all of the tests, the maximum stress and strain amplitude are recorded. Figure 6 shows peak tensile stress variation under strain controlled conditions. Representative hysteresis loops for this material under strain control are shown in Fig. 7.

Crack formation and growth in this nodular iron has been monitored by means of a cellulose acetate replicating procedure. Examination of the final surface replica resulted in the detection of major crack systems. The crack growth during the entire life could be reconstructed from the replica. Two representative examples are shown in Figs. 8 and 9. In Fig. 8, the crack was formed as in Fig. 8(a) and developed as in Fig. 8(b). The photographs in Fig. 8(b) and Fig. 9 show only a portion of the complete crack system. Other completed crack growth systems can be found in Refs. [7,8].

The longest crack in any crack system was used as the crack length. Crack length versus applied cycles data under load control mode is presented in Fig. 10. Strain control test results are shown in Fig. 11. Correlation of crack growth data with ΔJ are shown in Figs. 12 through 16. Figures 12 and 13 are cases which do not include material constant to correct short crack effects. When the material constant is included into crack length, the crack growth rate curves change to Fig. 14 and 15, respectively. When all of the data are plotted together, the crack growth data is as shown in Fig. 16. In Fig. 16, the solid line represents a linear regression analysis of the data. Finally, two examples of fracture surfaces are shown in Fig. 17.

6. DISCUSSION

This material showed substantial cyclic hardening during the entire life. The comparison of monotonic and cyclic stress-strain curve is made in Fig. 3. Since small cracks within 5 percent of the life could be detected, the load drop due to crack growth should occur from the very early time in case of cyclically stable material. However, by interacting with cyclic hardening, the load (stress) does not drop until the moment of final failure. At high strain amplitudes, stress levels do not stabilize. At lower strain amplitudes, the stress levels remain almost constant (see Fig. 6).

In Fig. 8(a), small cracks were seen to originate at irregular graphite which induce the most severe stress intensity. Once initiated, as Fig. 9 shows, cracks will propagate by linking with graphite nodules, other cracks and discontinuties.

Fracture surfaces were examined after the tests. The surface crack length developed from 4 mm to 8 mm depending on loading conditions. Generally at lower load levels, longer surface crack lengths are observed as Figs. 10 and 11. Since the response of the material was cyclic hardening interacting with crack growth, load drop prior to final fracture could not easily be detected even with computer control.

As Dowling [14] pointed out, the crack depth assumed based on a half-circular shape may have been in error. After examining all of the broken specimens, the ratio of surface crack length to depth was found be between 2.5 and 3.5. The ratio of three was used in this paper instead of half-circular assumptions.

The crack growth rates versus $(E\Delta J)^{1/2}$ data in Figs. 12 and 13 were formed without including short crack effects. In the figures, N is cyclic strain hardening exponent and A_0 was used as material constant. Both of the

curves show divergence at smaller cracks. By using the concept of the material constant [11], and estimating values of threshold stress intensity factor and fatigue limit, one could get better correlation as shown in Figs. 14 and 15. Compared with stress controlled data (Fig. 14), strain controlled data (Fig. 15) produces better correlation.

Although Fig. 15 shows better results, the divergence still exists at smaller crack lengths. This may be due to the effect of discontinuities in the material [19]. The decreasing and then increasing deviation in growth rate encountered as the crack grows through the region of the nodule appears to be a direct reflection of the change in localized stress caused by the presence of the nodule. As the crack approaches the back side of the nodule, the blunt nature of the nodule tends to retard cracking, subsequently reducing the rate of crack growth. Therefore, it appears that at least two interacting effects control the influence of discontinuities on fatigue crack growth behavior--localized stress effects and crack blunting effects. Also the specific influence of a given nodule (regard as internal defect) on the rate of fatigue crack growth depends upon the applied stress intensity level. The higher the stress intensity level, the smaller the influence of crack "blunting." This may be a positive statement while examining Fig. 15, divergence occurs almost at lower stress intensity level.

The scatterband of a factor 3 from the center solid line will include most of the data points as Fig. 16 shows. Thus, data from both stress control tests and strain control tests can be correlated with the ΔJ parameter.

7. CONCLUSIONS

The formation and growth of fatigue cracks has been monitored and fatigue data were correlated by the ΔJ parameter. Conclusions drawn from this work are:

(1) The origination of fatigue crack starts at the places which exhibit the highest stress intensifier. A few severe imperfections always exist in the material. Then cracks will initiate from those imperfections.

(2) Although the tensile properties of nodular iron are very close to steel, it exhibited different fatigue behavior. That is the detection of cracks at very early time in the life (less than 5 percent of the life) illustrate that the damage process is crack propagation. Hence, the study of fatigue behavior of cast irons should concentrate on crack growth.

(3) The divergence of crack growth rates at smaller crack regions may be due to the effect of discontinuities in the material.

(4) Both load-controlled tests and strain controlled tests may be correlated with the ΔJ parameter.

Table 1 Material Composition

C	Mn	S	P	Si	Cr	Ni	Mo	Cu	Mg
3.57	0.53	0.014	0.015	2.73	0.06	0.05	0.01	0.41	0.05

Table 2 Mechanical Properties

Young's Modulus (GPA)	164
Yield Strength, 0.2 Percent (MPA)	553
True Fracture Strength (MPA)	716
True Fracture Ductility	0.0413
Bulk Hardness (BHN)	235

Table 3 Stress-Life Data (R = -1)

Specimen No.	Δs/2 (MPA)	N_f
301	400	11320
302	350	60993
304	500	1284
305	300	147718
306	250	$>1.08 \times 10^6$
307	450	6154
311	400	20102
312	350	70015
313	450	8339
275	500	1467*
361	350	47503*
362	300	147808
372	400	20239*

* Crack growth test

Table 4 Strain-Life Data (R = -1)

Specimen No.	$\Delta\varepsilon/2$	N_f
373	0.002	1.0×10^5
392	0.002	57673*
391	0.0025	17159*
376	0.0025	20780
316	0.0025	26791
345	0.003	8548
396	0.003	6611
374	0.003	8956
381	0.003	8434*
314	0.004	1695
297	0.004	2116
395	0.004	2113
383	0.004	1655*
348	0.005	572
318	0.005	983
276	0.005	608
375	0.005	847

*Crack growth test

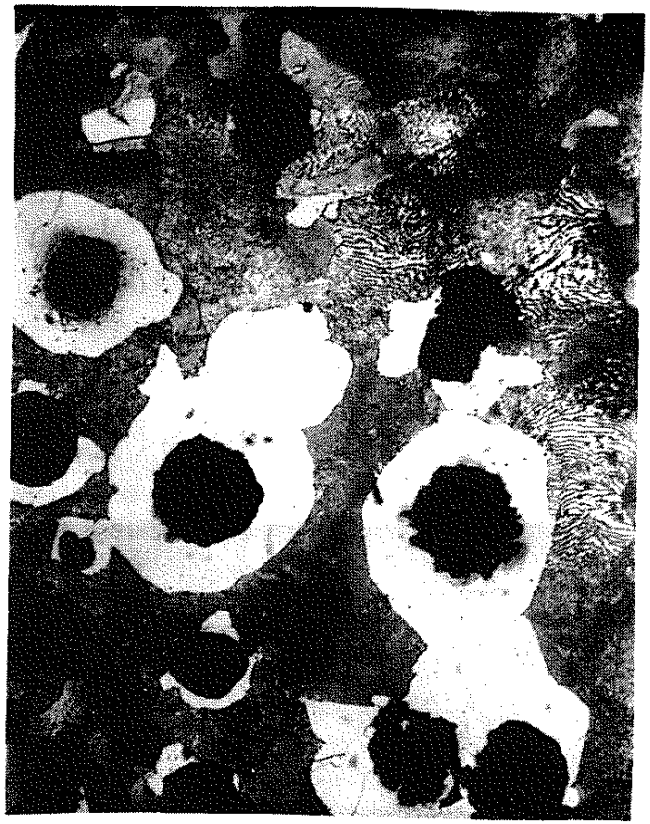

Pearlitic Nodular Iron,
2 Percent Nital (368X)

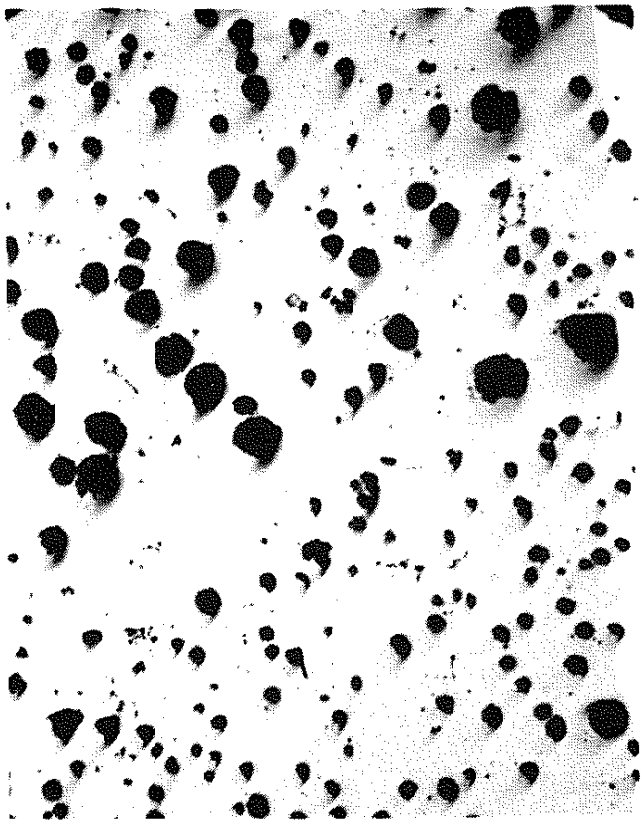

Size 5

Figure 1 Matrix Microstructure

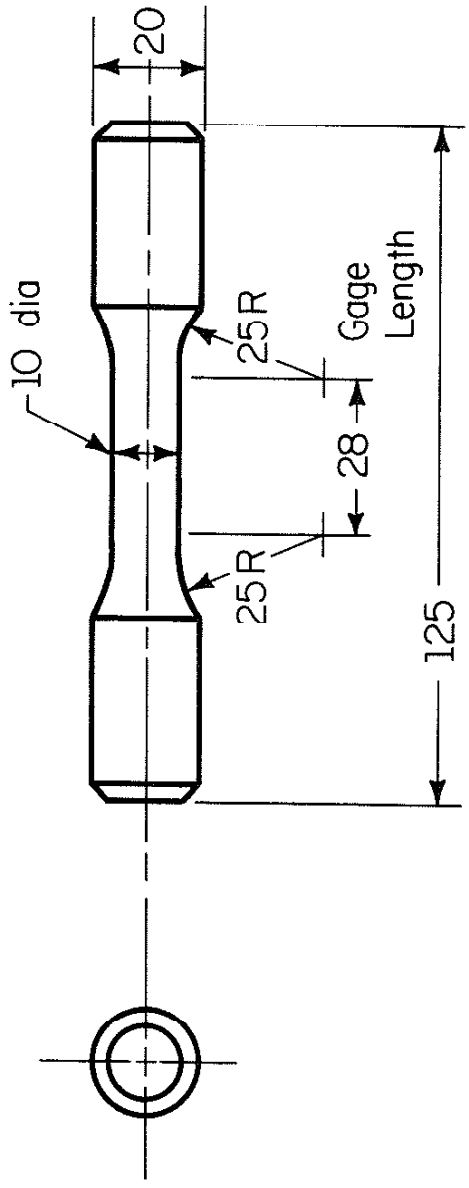

Figure 2 Test Specimen

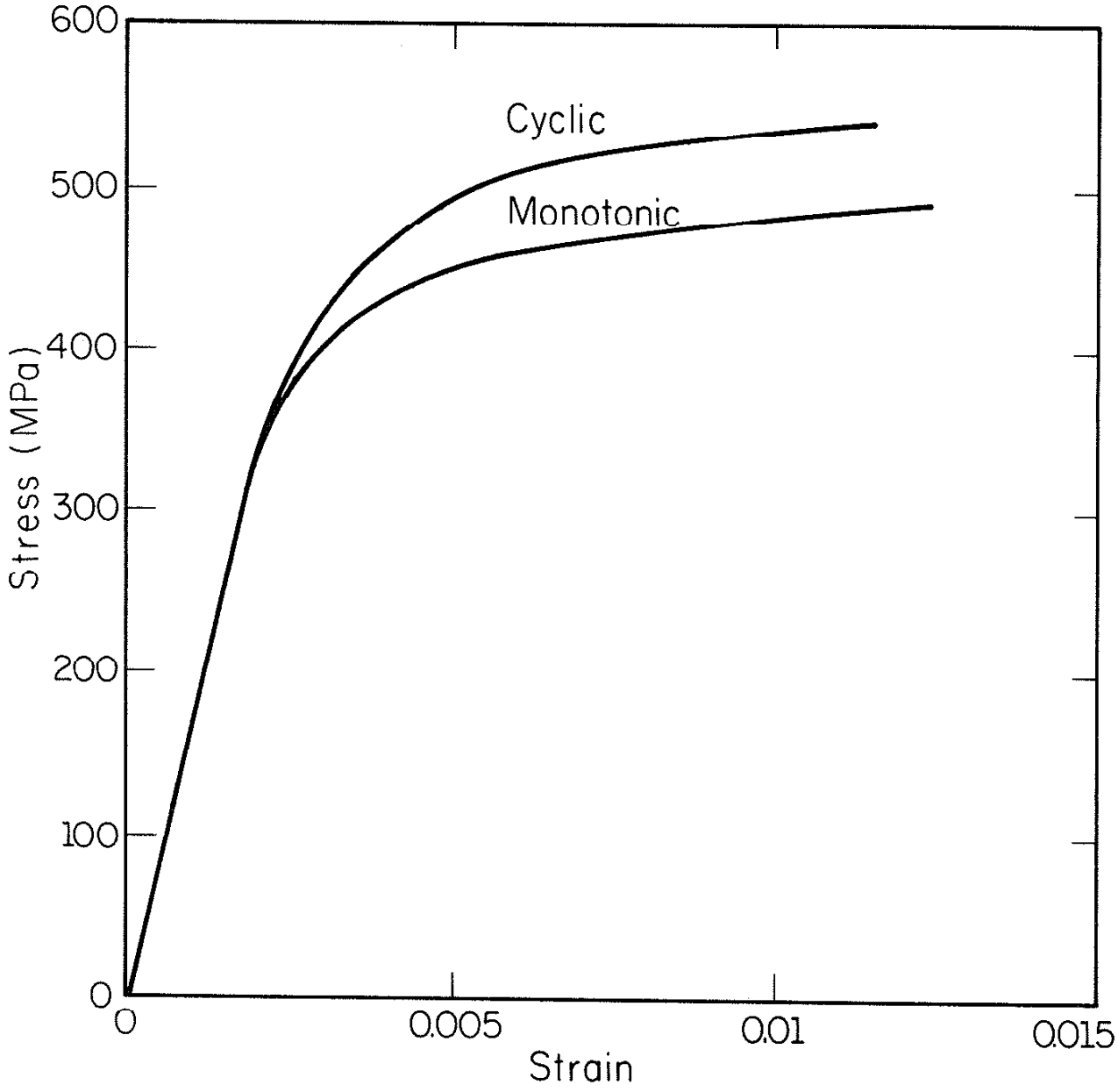

Figure 3 Monotonic and Cyclic Stress-Strain Curves

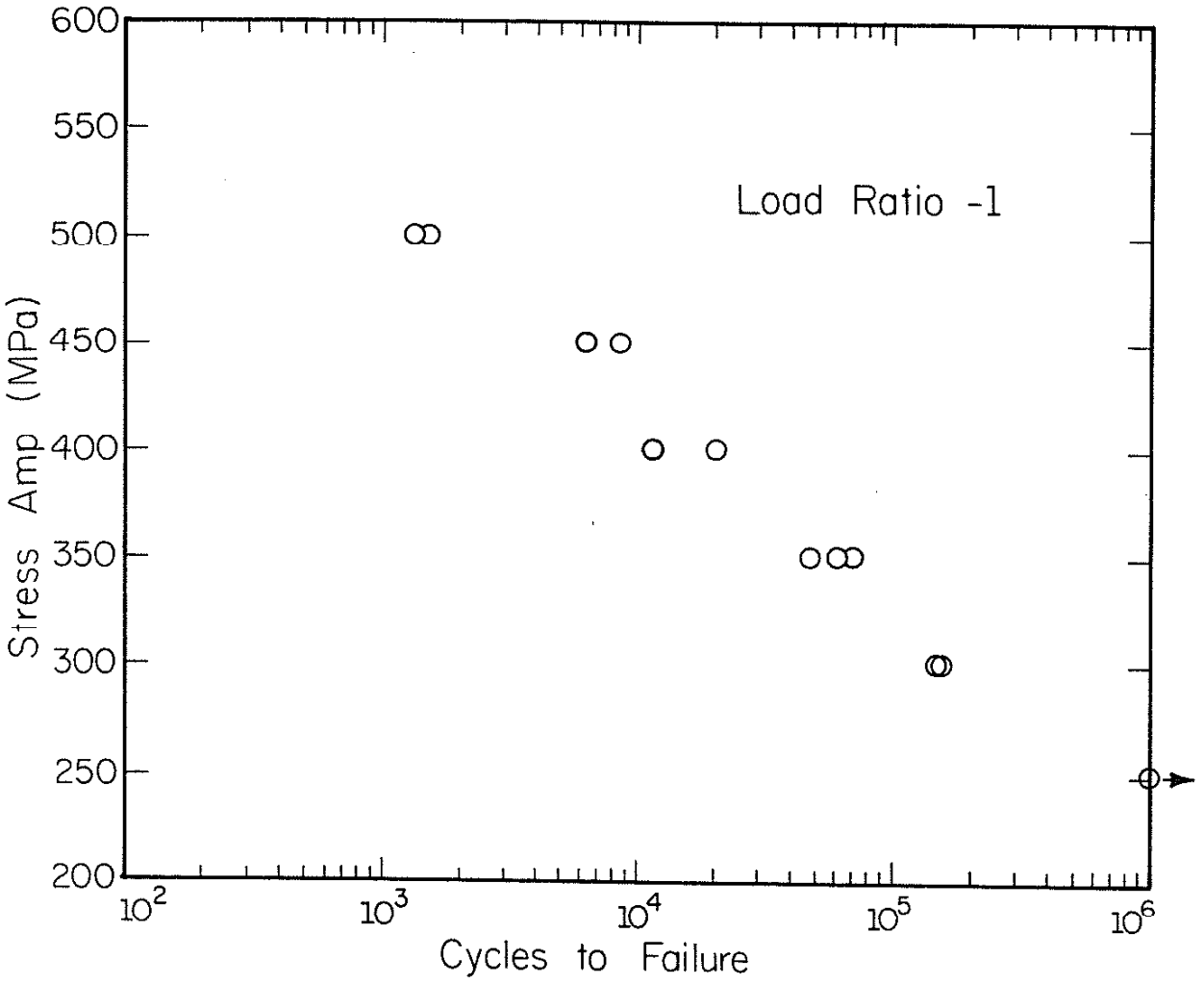

Figure 4 Stress versus Life Fatigue Curve

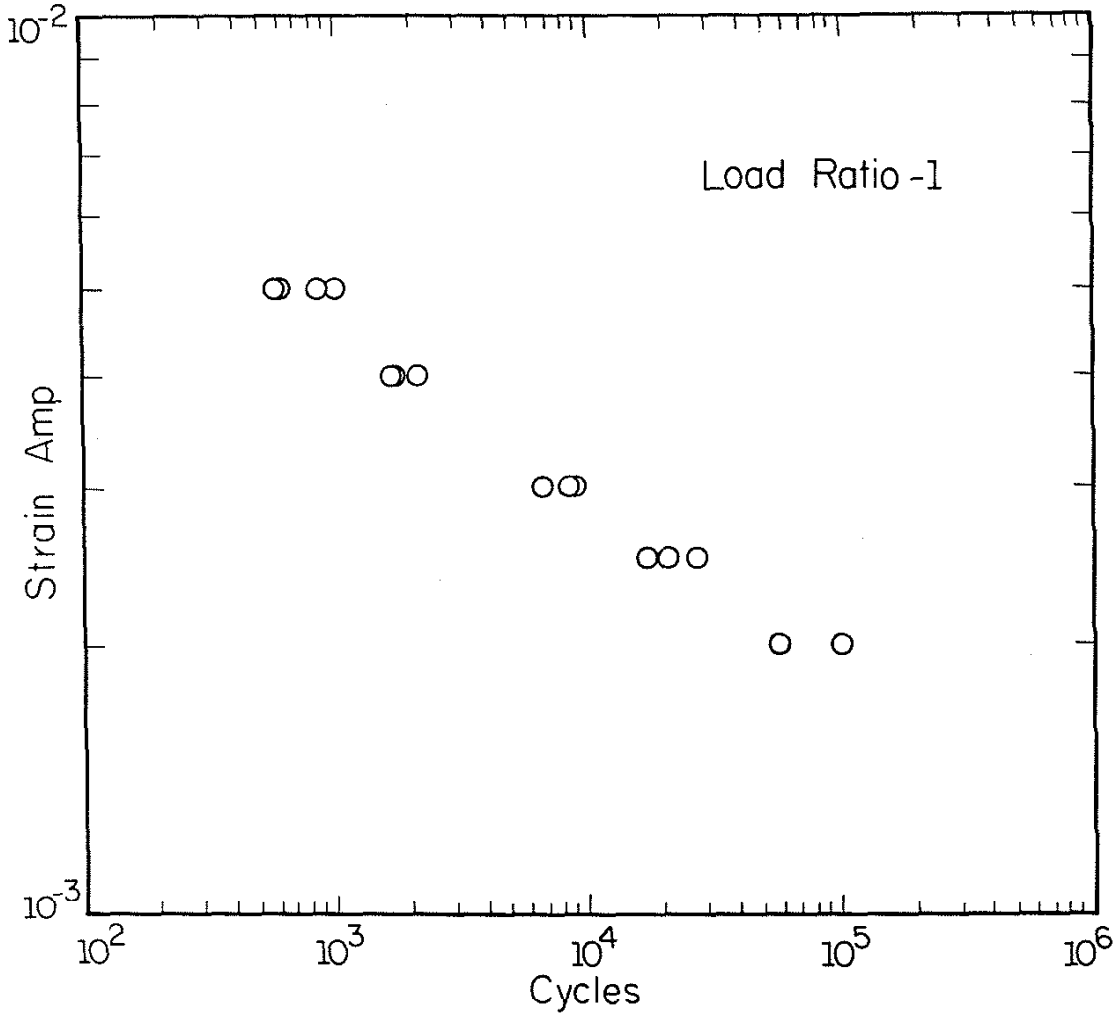

Figure 5 Strain versus Life Fatigue Curve

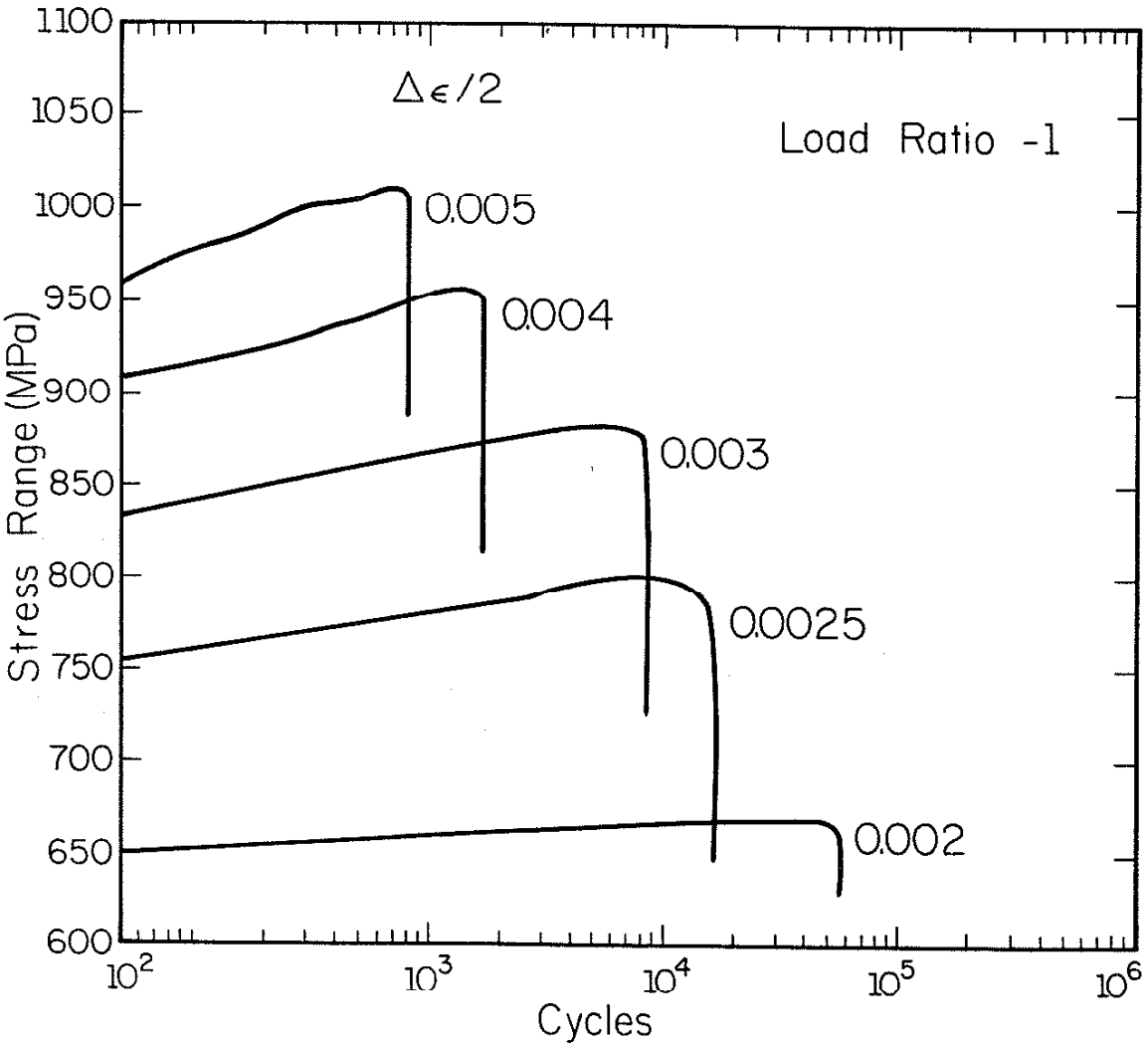

Figure 6 Stress Variation versus Applied Cycles (strain controlled)

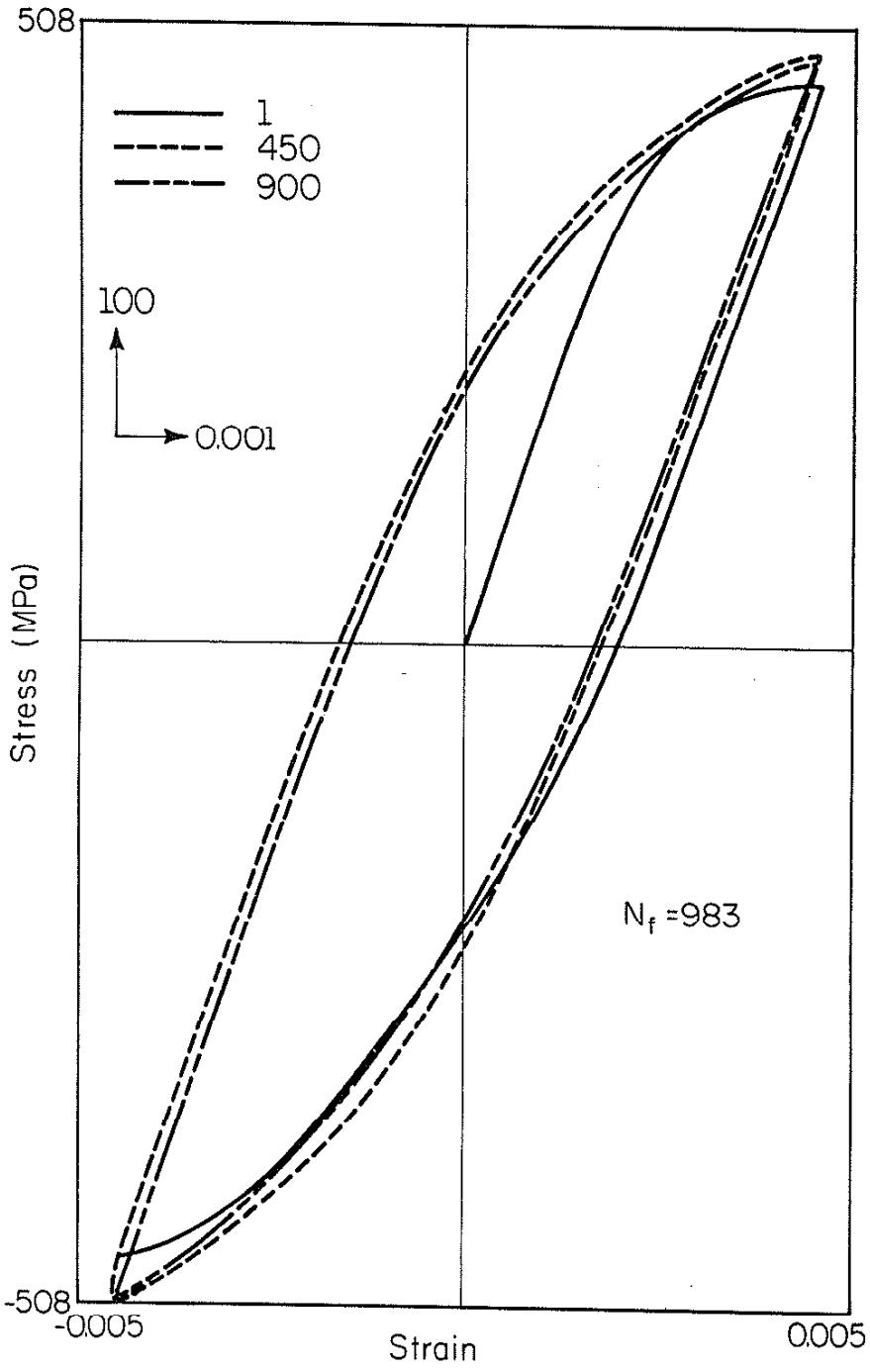

Figure 7 Hysteresis Loop (Strain Controlled)

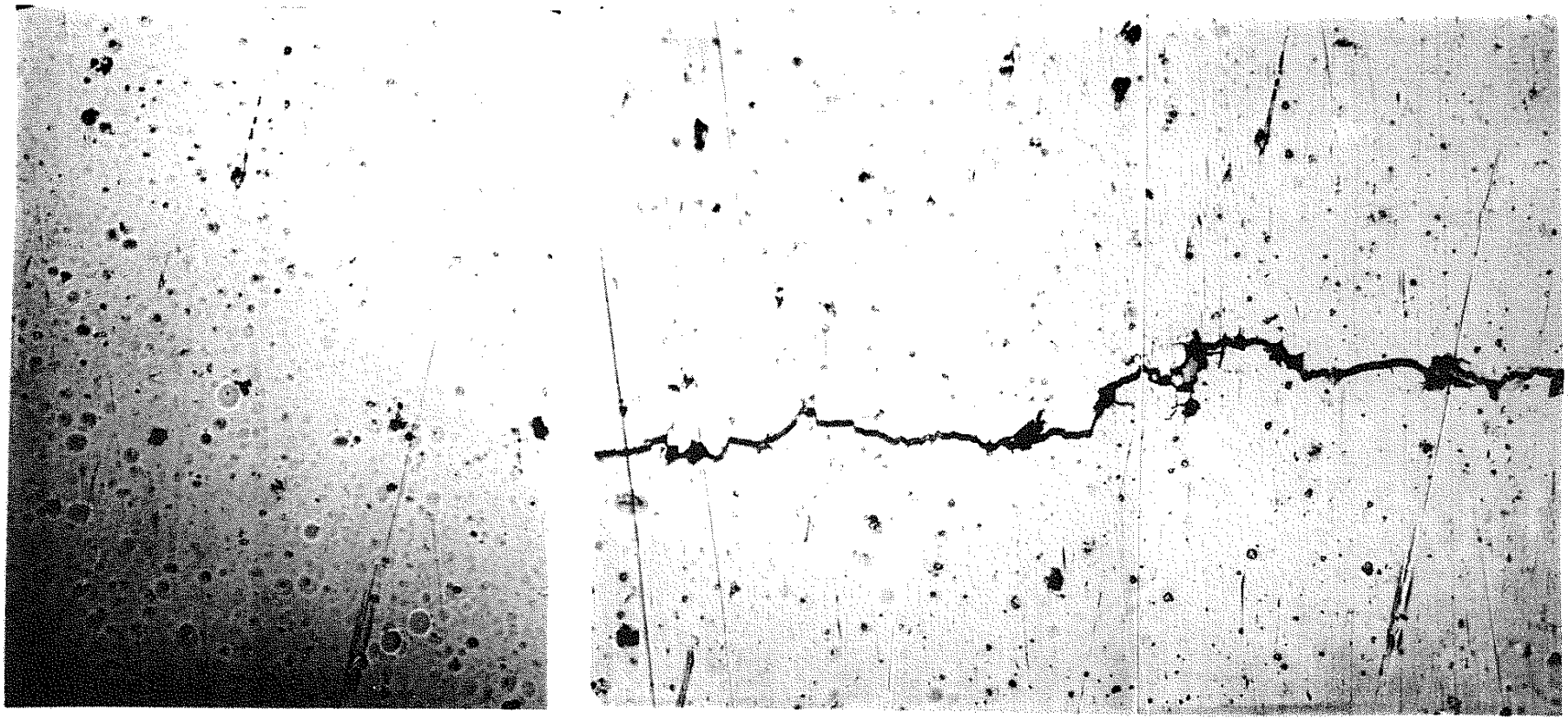

(a) N = 30

(b) N = 47,493

Figure 8 Crack Formation and Growth
(NI 361, N_f = 47,503, 100X)

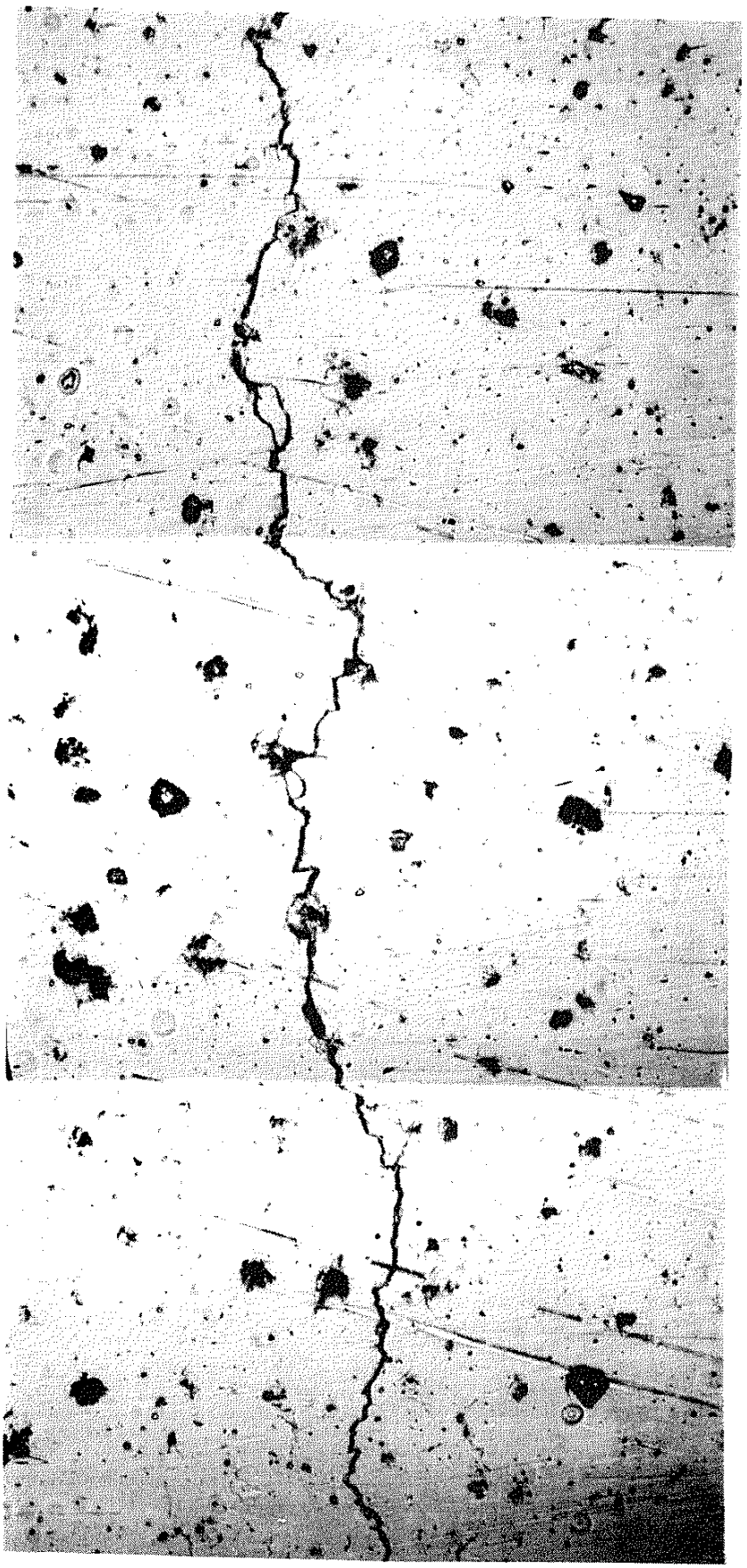

N = 20,198

Figure 9 Crack Growth in Nodular Iron (NI 372, N_f = 20,349, 100X)

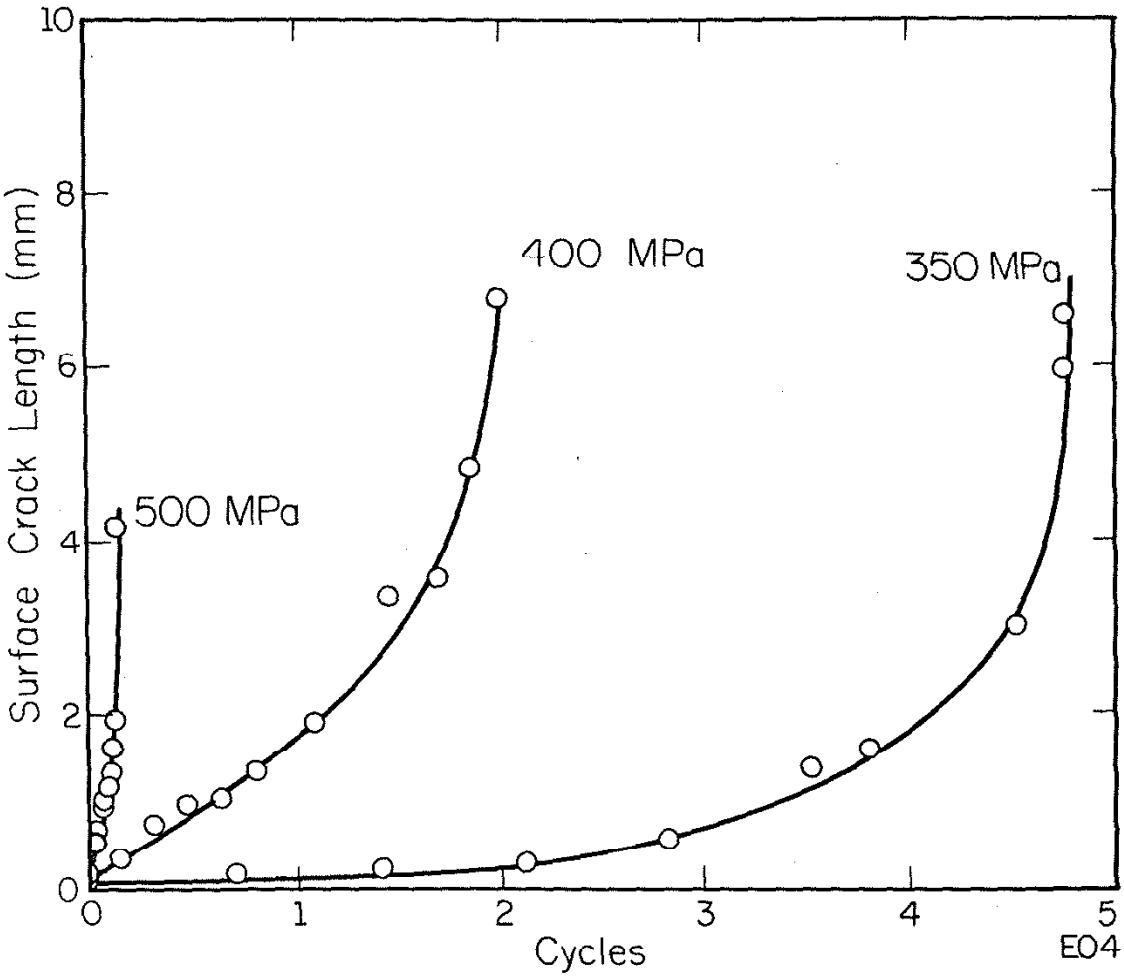

Figure 10 Stress Controlled Crack Growth Curve

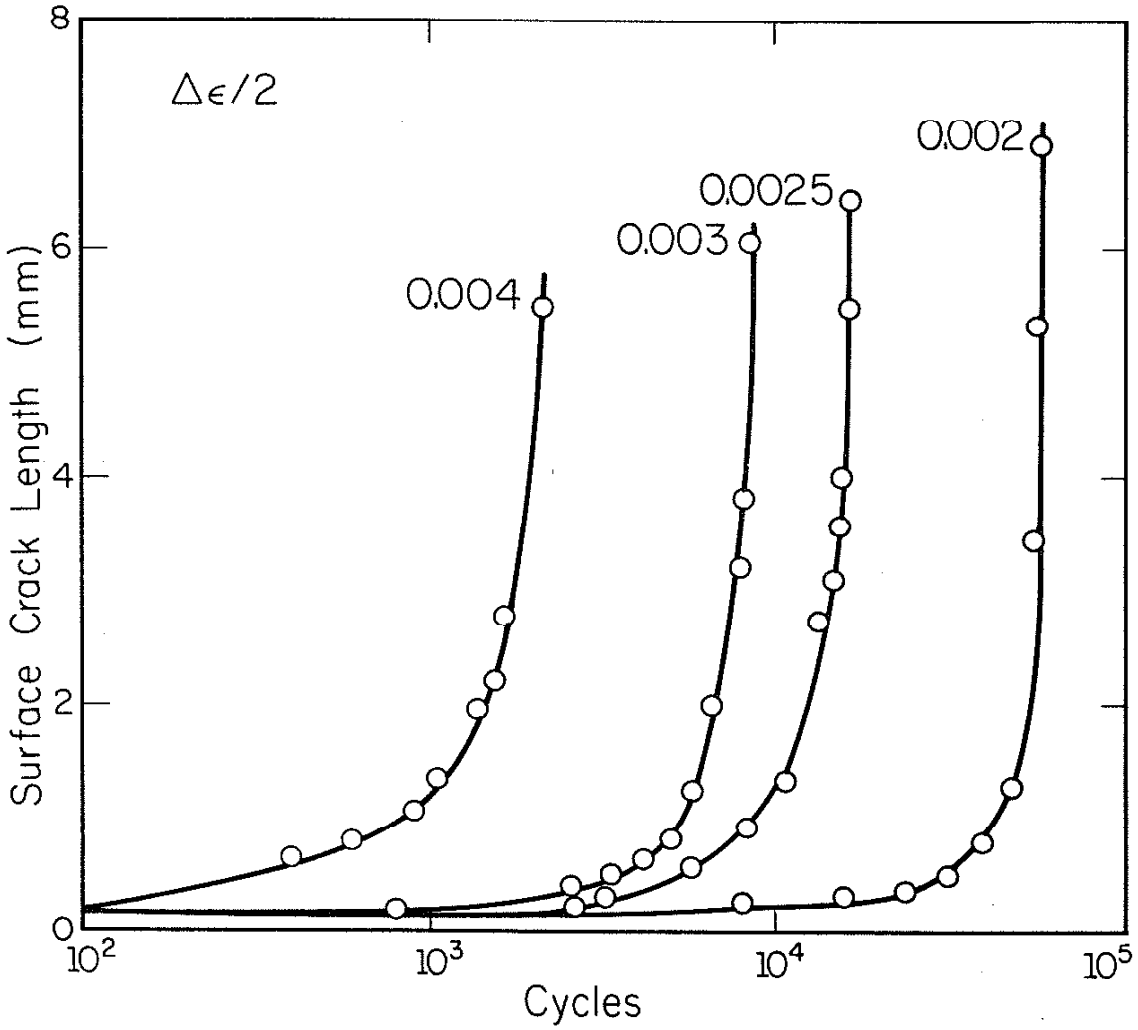

Figure 11 Strain Controlled Crack Growth Curve

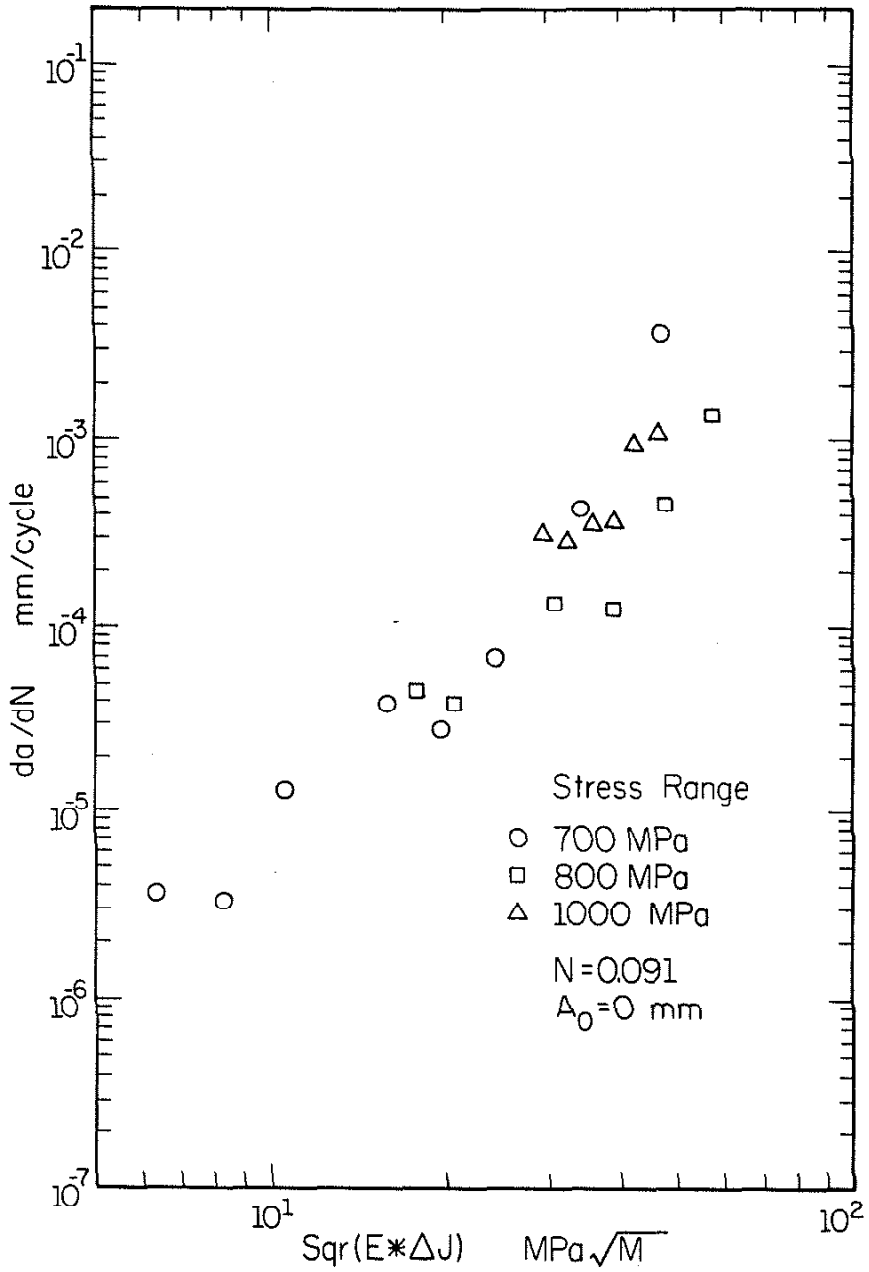

Figure 12 da/dN versus $(E\Delta J)^{1/2}$ Curve (Stress Controlled)

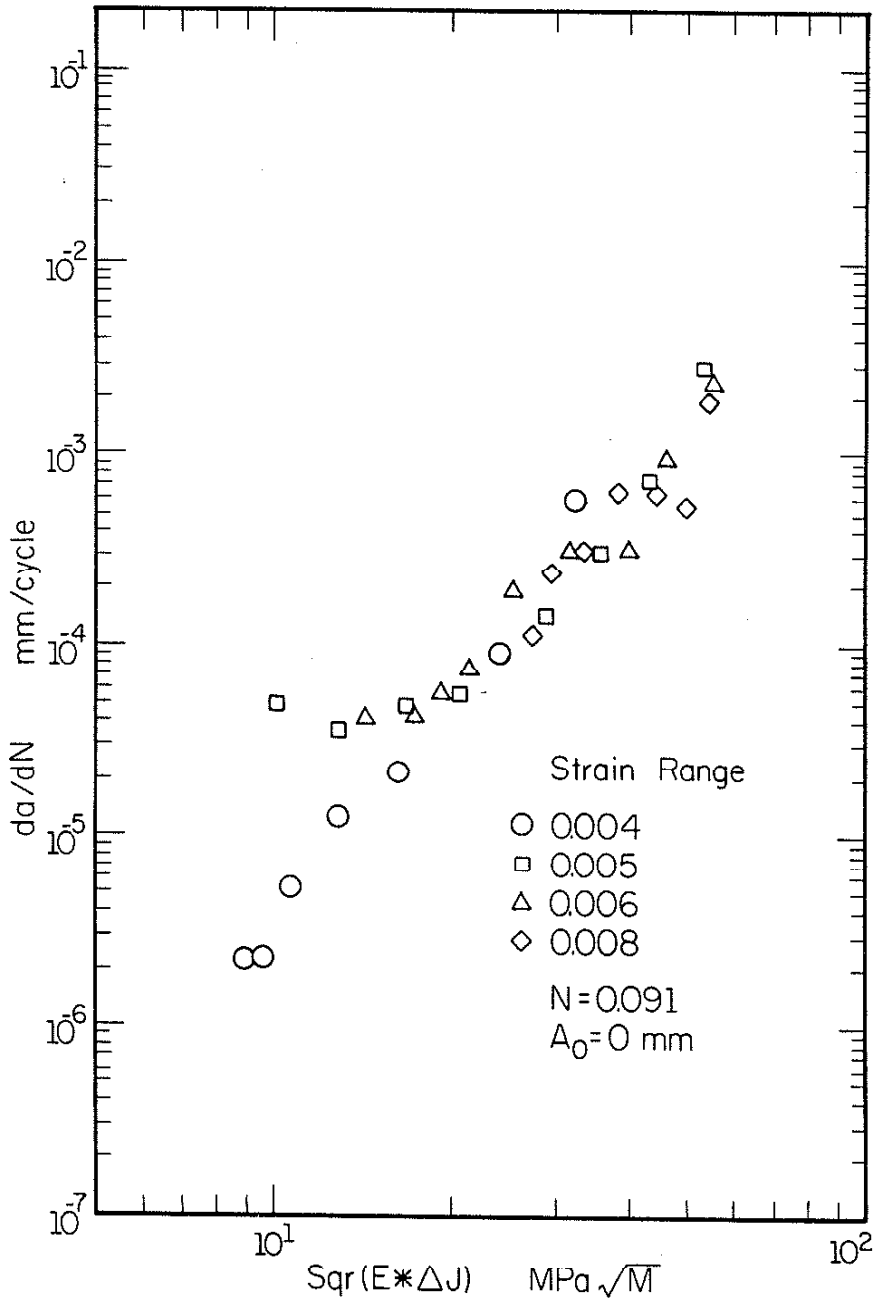

Figure 13 da/dN versus $(E\Delta J)^{1/2}$ Curve
(Strain controlled)

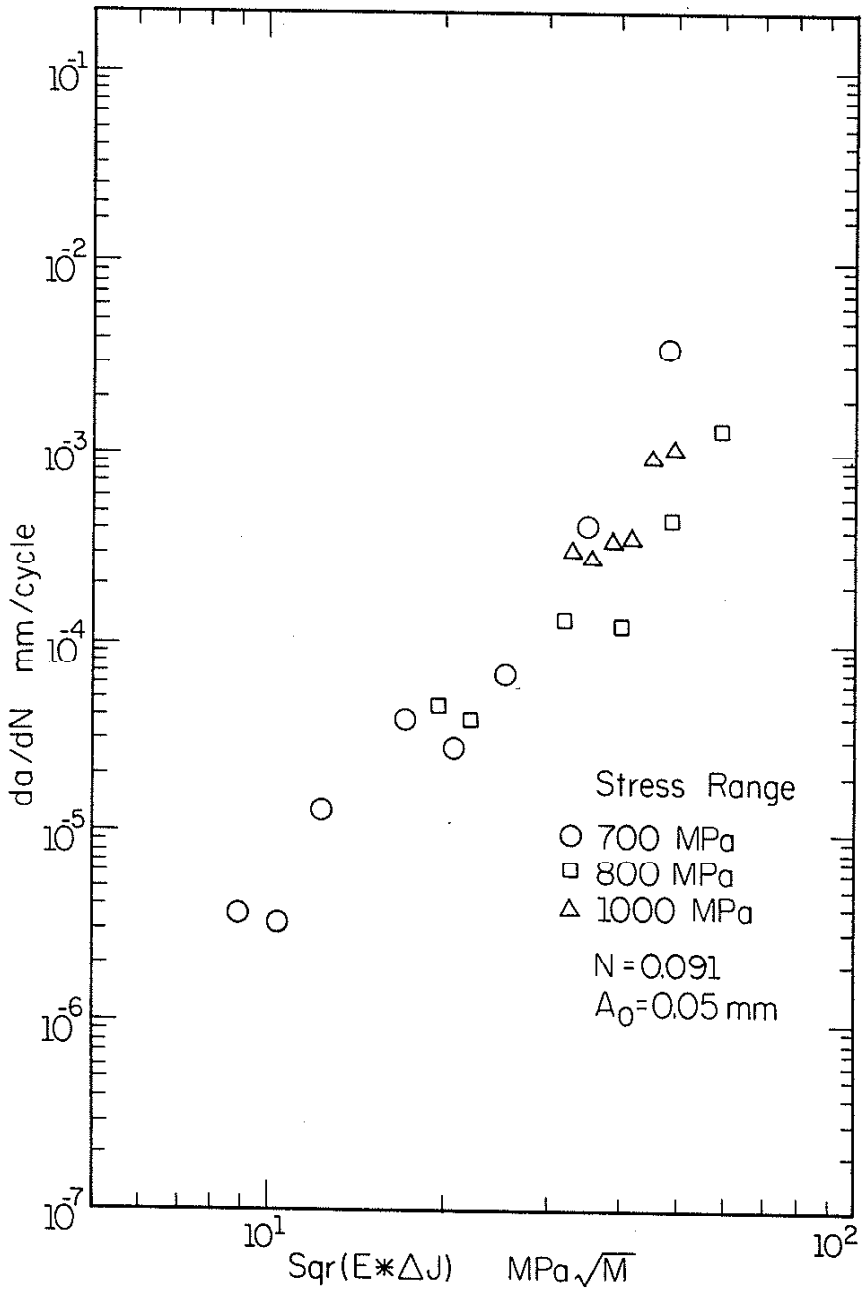

Figure 14 da/dN versus $(E\Delta J)^{1/2}$ Curve
(Stress Controlled)

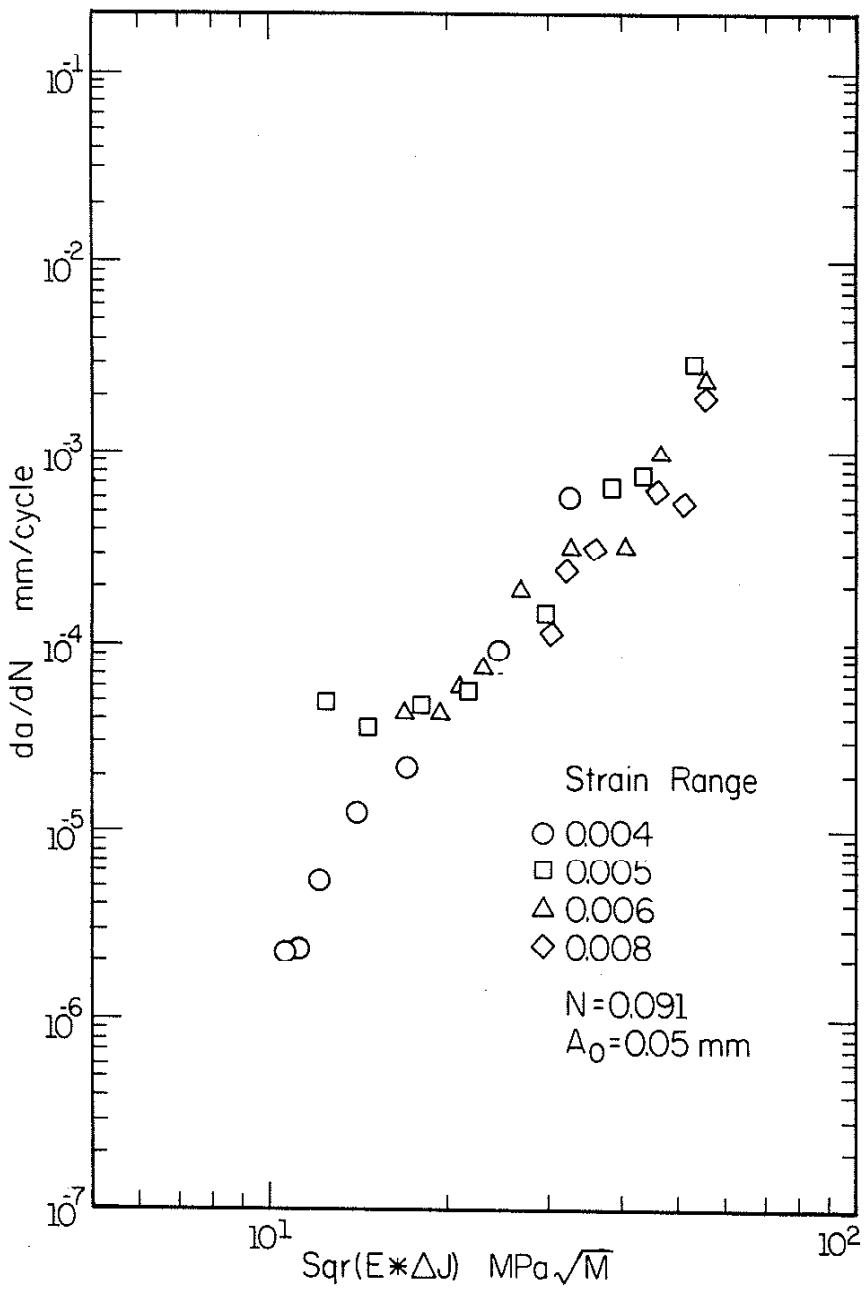

Figure 15 da/dN versus $(E\Delta J)^{1/2}$ Curve
(Strain Controlled)

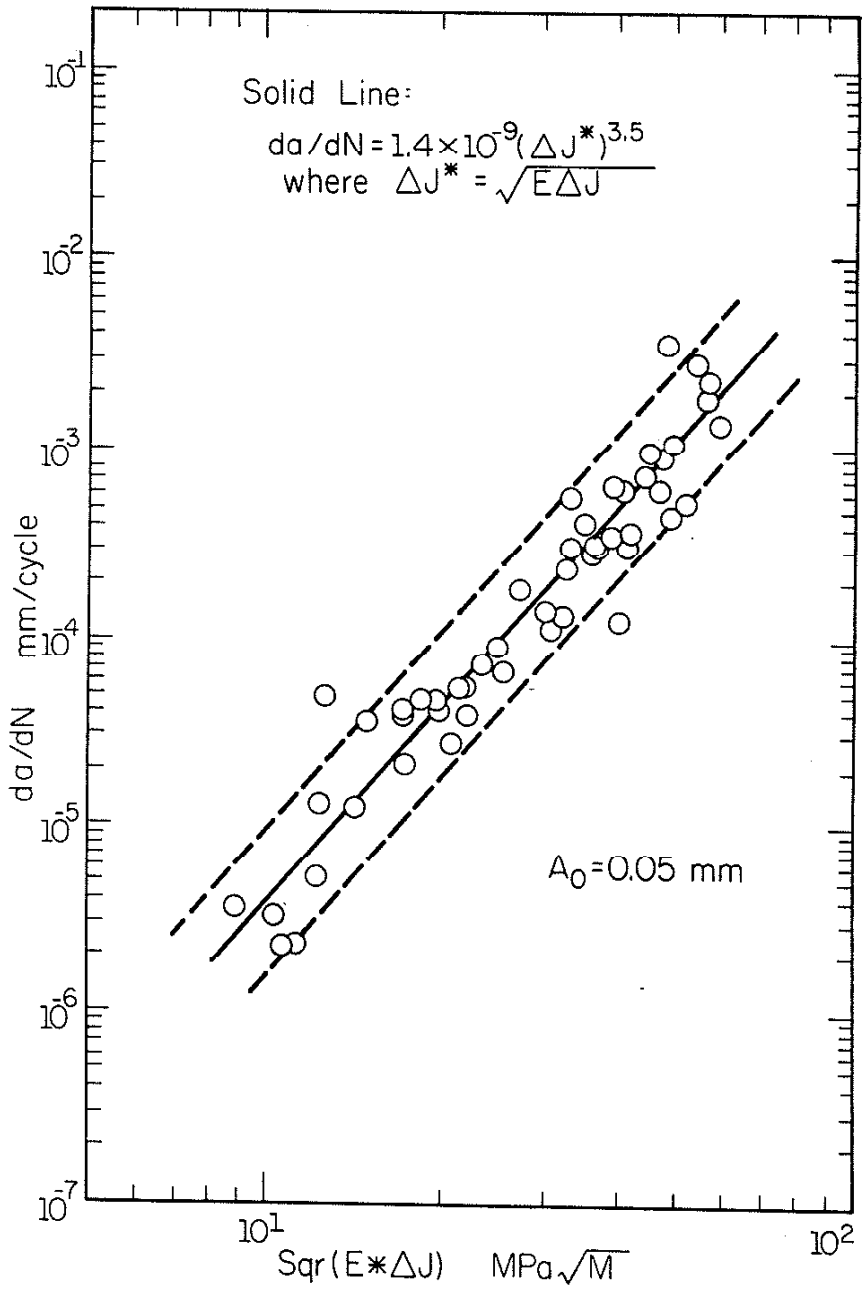

Figure 16 da/dN versus $(E\Delta J)^{1/2}$ Curve (Total Data)

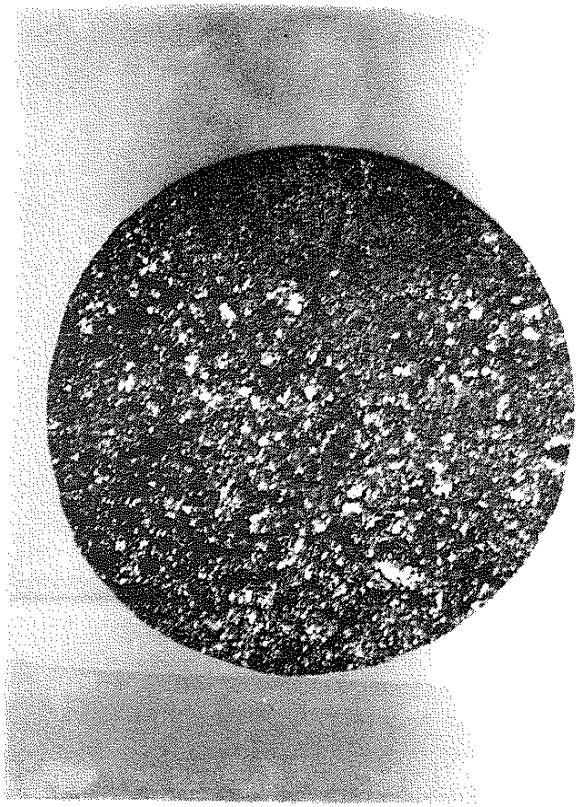

NI 312

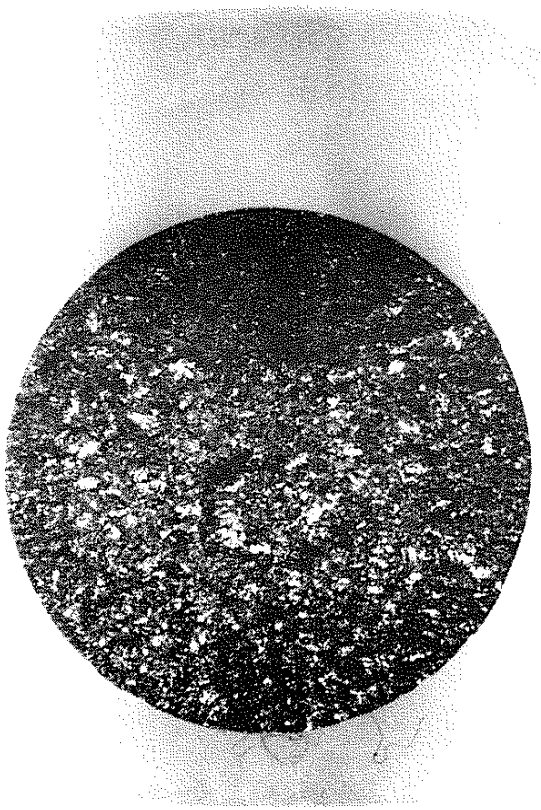

NI 362

Figure 17 Fracture Surfaces

REFERENCES

1. Millis, K. D., and A. P. Gagnebin, "Ductile Iron: Birth of a Giant," Nickel Topics, Vol. 26, No. 1, 1973, pp. 8-9.

2. Gilbert, G. N. J., "The Stress/Strain Properties of Nodular Cast Iron in Tension and Compression," J. BCIRA, Vol. 12, No. 2, 1964, pp. 170-193.

3. Ikawa, K., and G. Ohira, "Fatigue Properties of Cast Iron in Relation to Graphite Structure," AFS, Cast Metals Research J., Vol. 3, 1967, pp. 11-21.

4. Testin, R. A., "Characterization of the Cyclic Deformation and Fracture Behavior of Nodular Cast Iron," TAM Report No. 371, University of Illinois at Urbana-Champaign, 1973.

5. Fuller, A. G., "Effect of Graphite Form on Fatigue Properties of Pearlitic Ductile Irons," AFS Trans., Vol. 85, 1977, pp. 527-536.

6. Mitchell, M. R., "A Unified Predictive Technique for the Fatigue Resistance of Cast Ferrous-based Metals and High Hardness Wrougth Steels," FCP No. 23, 1976.

7. Fash, J. W., "Fatigue Crack Initiation and Growth in Gray Cast Iron," FCP No. 35, 1980.

8. Molinaro, L., "Fatigue Behavior and Crack Development in Compacted Graphite Cast Iron," FCP No. 39, 1981.

9. Starkey, M. S., and P. E. Irving, "The Influence of Microstructure on fatigue Crack Initiation in Spheroidal Graphite Cast Iron," GKN Technical Report, GKN Group Technological Centre, Wolverhampton, England, 1979.

10. Shih, C. F., and J. W. Hutchinson, "Fully Plastic Solutions and Large Scale Yielding Estimates for Plane Stress Crack Problems," J. of Engr. Material and Technology, Trans. of ASME, 1976, pp. 289-295.

11. El. Haddad, M. H., et al., "Fatigue Crack Propagation of Short Cracks," J. of Engr. Material and Technology, Vol. 101, 1979, pp. 42.

12. Paris, P. C., and F. Erdogen, "A Critical Analysis of Crack Propagation Laws," J. Basic Engr., Trans. ASME, Vol. 85, 1963, pp. 528.

13. Rice, J. R., "A Path Independent Integral and Approximate Analysis of Strain Concentration by Notches and Cracks," J. Applied Mechanics, 1968, pp. 379-386.

14. Dowling, N. E., "Crack Growth during Low-Cycle Fatigue of Smooth Axial Specimens," ASTM STP 637, 1977, pp. 97-121.

15. Paris, P. C., "Fracture Mechanics in the Elastic-Plastic Regime," ASTM STP 631, pp. 3-27.

16. Shih, C. F., in "Mechanics of Crack Growth," ASTM STP 590, 1976, pp. 3-26.

17. Begley, J. A., et al., "An Estimation Model for the Application of the J-Integral," ASTM STP 560, 1974, pp. 155-169.

18. Paris, P. C., and G. C. Sih, ASTM STP 381, 1965, pp. 30-83.

19. Clark, W. G., "Effect of Spherical Discontinuities on Fatigue Crack Growth Rate Performance," ASTM STP 677, 1979, pp. 301-319.

PARTIAL LIST OF FRACTURE CONTROL PROGRAM REPORTS

REPORT NO.

29 "THE EFFECT OF RESIDUAL STRESSES ON WELD FATIGUE LIFE," J. D. BURK AND F. V. LAWRENCE, JANUARY, 1978.

30 "CHARACTERIZATION OF DUCTILE FRACTURE IN WROUGHT STEELS AND WELDMENTS," E. P. COX, F. V. LAWRENCE AND G. M. SINCLAIR, JUNE, 1978.

31 "EFFECT OF SPECTRUM EDITING ON FATIGUE CRACK INITIATION AND PROPAGATION IN A NOTCHED MEMBER," DARRELL F. SOCIE AND PAUL J. ARTWOHL, DECEMBER, 1978.

32 "A MODEL FOR JOINING THE FATIGUE CRACK INITIATION AND PROPAGATION ANALYSES," W.-C. CHEN AND F. V. LAWRENCE, NOVEMBER, 1979.

33 "FINITE ELEMENT SIMULATION OF THE MICROSTRUCTURE OF GRAY CAST IRON," EDWARD S. RUSSELL, DECEMBER, 1979.

34 "CYCLIC DEFORMATION AND FATIGUE BEHAVIOR OF CARBURIZED STEEL," JOHN M. WARANIAK, MAY, 1980.

35 "FATIGUE CRACK INITIATION AND GROWTH IN GRAY CAST IRON," JAMES W. FASH, OCTOBER, 1980.

36 "PREDICTING THE FATIGUE RESISTANCE OF WELDS," F. V. LAWRENCE, N.-J. HO AND P. K. MAZUMDAR, OCTOBER, 1980.

37 "CYCLE COUNTING FOR VARIABLE AMPLITUDE CRACK GROWTH," DARRELL F. SOCIE AND PETER KURATH, APRIL, 1981.

38 "AN ANALYTICAL STUDY OF THE FATIGUE NOTCH SIZE EFFECT," P. K. MAZUMDAR AND F. V. LAWRENCE, APRIL, 1981.

39 "FATIGUE BEHAVIOR AND CRACK DEVELOPMENT IN COMPACTED GRAPHITE CAST IRON," LAWRENCE MOLINARO, MAY, 1981.

40 "FATIGUE OF LOW CARBON STEELS AS INFLUENCED BY REPEATED STRAIN AGING," HUSEYIN SEHITOGLU, JUNE, 1981.

41 "AXIAL CYCLIC RESPONSE OF UNNOTCHED AND NOTCHED CARBURIZED CYLINDRICAL MEMBERS UNDER CONSTANT AMPLITUDE COMPLETELY REVERSED LOADING," GOLAM M. NEWAZ, NOV., 1981.

42 "THE EFFECT OF SELECTED SUBCYCLES IN BLOCK LOADING FATIGUE HISTORIES," THOMAS J. DEVES, PETER KURATH, HUSEYIN SEHITOGLU AND JODEAN MORROW, MARCH, 1982.

43 "LOW CYCLE TORSIONAL FATIGUE OF 1045 STEEL IN SHEAR STRAIN CONTROL," GAIL E. LEESE, SEPTEMBER, 1982.

44 "FATIGUE OF GRAY IRON," D. F. SOCIE, J. W. FASH AND S. D. DOWNING, OCTOBER, 1982.

45 "THE FATIGUE OF WELDMENTS SUBJECTED TO COMPLEX LOADINGS," N.-J. HO AND F. V. LAWRENCE, JANUARY, 1983.

46 "IMPROVEMENT OF WELD FATIGUE RESISTANCE," S.-T. CHANG AND F. V. LAWRENCE, JANUARY, 1983.